A&A 375, 100–112 (2001)
DOI: 10.1051/0004-6361:20010823

Astronomy & Astrophysics

New physical elements of HR 7428 and its Hα behaviour*

G. Marino[1], S. Catalano[2], A. Frasca[2], and E. Marilli[2]

[1] Telescopio Nazionale Galileo, Calle Alvarez de Abreu 70, 38700 Santa Cruz de La Palma (TF), Canary Island, Spain
[2] Osservatorio Astrofisico di Catania, via S. Sofia 78, 95123 Catania, Italy

Received 7 February 2001 / Accepted 28 May 2001

Abstract. HR 7428 is a spectroscopic binary composed of a K2 II-III and a main-sequence A2 star. Thanks to a new set of radial velocity measurements from our and IUE spectroscopy we have improved the orbital period determination and the spectroscopic elements of both components. Combining optical photometry and UV low dispersion IUE spectra we have determined new stellar parameters through photospheric synthetic spectra using the NextGen models by Hauschildt et al. (1999a, 1999b). The hot secondary component parameters agree with those of a typical A2 V star while the radius of the primary cool star turns out to be 40 $R_\odot$, i.e. significantly smaller than a previous estimate of 62 $R_\odot$. The position of the hot and cool component on the H–R diagram is consistent with a normal evolution, without any mass exchange, of this binary system, whose age is in the range 100–200 Myrs. The system displays a filled-in Hα profile with significant variations both in depth and width along the orbital phase. In addition to the Hα chromospheric emission component, we have detected, at some phases, a broad extra-absorption and emission that we relate to an inter-system cloud.

Key words. stars: activity – stars: binaries: spectroscopic – stars: individual: HR 7428

1. Introduction

HR 7428 (=V 1817 Cygni) is a spectroscopic binary composed of a K2 II-III star (Ginestet et al. 1999) and a main sequence A2 star (Parsons & Ake 1987). Its long orbital period (≃108.6 days) has probably prevented systematic spectroscopic observations in the last decades. So, before the present work, the only available spectroscopic observations and orbital solution, for the primary cool component, have been done by Sanford (1925). Lucy & Sweeney (1971) revised that solution and concluded that the eccentricity is not significantly different from zero.

Ca II H & K emission was first reported by Gratton (1950), while Bopp & Talcott (1978) observed the Hα line in absorption. Xue-fu & Hui-song (1986a) detected emission in both Hα wings, but two later observations (Xue-fu & Hui-song 1986b) showed only variations in the Hα profile without any emission. A single spectrum presented by Eker et al. (1995) showed a filled-in Hα line. This observed behaviour indicates a large variability, probably due to chromospheric activity.

Barksdale et al. (1985) showed the system to be photometrically variable, the dominant cause being ellipticity, with a possible small reflection effect. Strassmeier et al. (1989) excluded reflection and estimated a starspot wave amplitude of 0.02 magnitudes from unequal heights of maxima and depths of minima in the light curve. A determination of physical parameters was performed by Hall (1990) combining the amplitude of the ellipticity effect, the mass function and the $v \sin i = 21$ km s^{-1} reported by Hui-song & Xue-fu (1987). A more recent and precise measurement of the projected rotational velocity, $v \sin i = 17.2 \pm 1.0$ km s^{-1}, has been provided by De Medeiros & Mayor (1995).

Photometric observations between 1982 and 1989 were used by Hall et al. (1990a) for a detailed analysis of the photometric behaviour. After removing the modulation produced by the ellipticity effect, they were able to detect starspot signatures on the K-type primary star, as well as migration of spots. Gurzadyan (1997) included HR 7428 in his sample of binary stars for which he estimated the radii of the main components in the hypothesis of common chromospheres around binary systems.

In this work we present the results of our optical spectroscopy and determine new orbital and physical parameters. We estimate new temperatures and radii of both components comparing UBV magnitudes and low resolution IUE spectra with synthetic photospheric spectra. The Hipparcos photometry is also discussed, to constrain the ellipticity parameters.

Send offprint requests to: A. Frasca,
e-mail: afr@sunct.ct.astro.it

* Based on observations collected at the Catania Astrophysical Observatory, Italy.

2. Hα observations and reduction

Spectroscopic observations have been performed with the échelle spectrograph at the 91-cm telescope of Catania Astrophysical Observatory – *M. G. Fracastoro* station (Serra La Nave, Mt. Etna) – in 1997, 1998, and 1999.

The spectrograph is fed by the telescope through an optical fiber (UV − NIR, 200 μm core diameter) and is placed in a stable position in the room below the dome level. Spectra were recorded on a CCD camera equipped with a front-illuminated CCD of 800× 1152 pixels (pixel size of 22.5 μm) in 1997-98 and with a thinned back-illuminated SITe CCD of 1024× 1024 pixels (size 24 × 24 μm) in 1999. With the first detector we were able to record four orders in each frame, spanning from about 6050 to 6650 Å, and to cover nearly completely each échelle order. With the second one we could record five échelle orders, starting from 5850 Å. The echelle cross-configuration yields a resolution of about 14 000, as deduced from the *FWHM* of the lines of the Th–Ar calibration lamp.

The average signal-to-noise ratio (S/N) obtained at the continuum near the Hα line was about 150.

The data reduction was performed by using the ECHELLE task of IRAF[1] package following the standard steps: background subtraction, division by a flat field spectrum given by a halogen lamp, wavelength calibration using the emission lines of a Thorium-Argon lamp, normalization through a polynomial fit to the continuum.

3. Orbital and physical parameters of the components

3.1. Radial velocities and orbital parameters

Radial velocity determinations were made by cross-correlation of each order of the HR 7428 spectra with spectra of the bright radial velocity standard star α Ari, whose radial velocity is -14.3 km s^{-1} (Evans 1979).

Template spectra of α Ari have been obtained during each observing run. From several spectra of α Ari and other *RV* standard stars we have evaluated an average accuracy for the radial velocity measurements better than ± 0.4 km s^{-1} rms which is the result of the stability of the experimental apparatus and is consistent with the limits given by the spectral resolution.

The wavelength ranges for the cross-correlation of HR 7428 spectra were selected in order to exclude the Hα and Na I D_2 lines, which are contaminated by chromospheric emission. The spectral regions heavily affected by telluric lines (e.g. the λ 6276−λ 6315 band of O_2) were also excluded.

Each radial velocity value listed in Table 1 is the weighted mean of the values obtained by the cross-correlation of each order of the target spectra with the corresponding order of the closest-in-time spectrum of α Ari. The errors, listed in Table 1, have been computed as the square root of the quadratic average of errors in the cross correlation of each order. The latter are computed according to the fitted peak height and the antisymmetric noise as described by Tonry & Davis (1979). This error estimate is consistent with the dispersion of data points around the mean curve.

Hall et al. (1990a), from Sanford's (1925) data set, redetermined the elements for a circular orbit and derived $JD_0 = 2423455.2 \pm 0.20$ as the time of conjunction (primary in front). From their own light curve (dominated by ellipticity effect) they deduced a time of conjunction $JD_0 = 2445988.0 \pm 0.3$. Combining the photometric and spectroscopic epoch of conjunction, Hall et al. (1990a) derived a period of 108.854 days. This value is slightly different from that given by Sanford (1925) of 108.57 days but very similar to the one they deduced from Fourier analysis of V band photometry (108.83 days).

If we use the above-mentioned ephemeris of Hall et al. (1990a) to fold in phase our radial velocities, the time of conjunction (primary star in front) occurs at phase $\phi = 0.64$, indicating that the period and/or the time of conjunction are not correct.

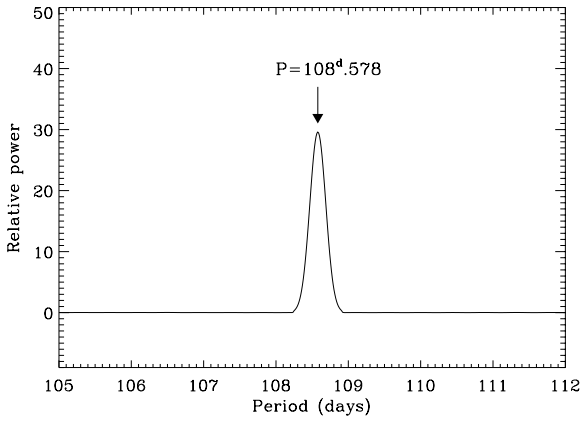

Fig. 1. The cleaned periodogram of our and literature *RV* data. The peak corresponds to a period of 108.578 days.

Radial velocities available from the literature (excluding the poor-quality five measures of Xue-fu & Hui-song 1986a) and our own data have been analysed applying the periodogram technique (Scargle 1982). The CLEAN iterative deconvolution algorithm (Roberts et al. 1986) has been used to eliminate the effects of the data sampling introduced by the observation spectral window in the power spectrum. The maximum of the power spectrum, plotted in Fig. 1, yields a period of 108.578 days, very close to Sanford's estimate. The new ephemeris we obtain is

$$T_{\rm conj} = 2450601.982 + 108.578\,n, \qquad (1)$$

where the epoch refers to the conjunction with the primary star in front.

[1] IRAF is distributed by the National Optical Astronomy Observatory, which is operated by the Association of University for Research in Astronomy, inc. (AURA) under cooperative agreement with the National Science Foundation.

Table 1. Radial velocities and Hα equivalent widths of HR 7428.

HJD −2400000	Phase	RV ($\mathrm{km\,s^{-1}}$)	error	$EW^{\mathrm{abs}}_{\mathrm{H}\alpha}$ (Å)	error	$EW^{\mathrm{net}}_{\mathrm{H}\alpha}$ (Å)	error
50631.5584	0.2724	17.9	1.0	−1.463	0.108	0.112	0.119
50632.5635	0.2817	19.3	0.4	−1.674	0.097	−0.255	0.107
50633.5440	0.2907	18.3	1.0	−1.686	0.181	−0.228	0.200
50634.5728	0.3002	15.7	0.5	−1.940	0.120	−0.558	0.132
50635.5511	0.3092	16.0	1.4	—	—	—	—
50636.5153	0.3181	15.9	2.8	−1.921	0.076	−0.432	0.084
50678.4853	0.7046	−29.8	0.7	−0.656	0.102	0.757	0.112
50679.4757	0.7137	−30.2	0.3	−0.784	0.071	0.676	0.078
50680.4779	0.7229	−30.0	1.3	−0.759	0.124	0.655	0.137
50681.5193	0.7325	−30.5	0.9	−0.905	0.097	0.481	0.107
50982.5670	0.5052	−7.2	0.7	−0.813	0.120	0.510	0.132
50992.5589	0.5972	−20.0	1.3	−0.918	0.128	0.473	0.141
51000.5715	0.6710	−27.8	0.5	−1.146	0.121	0.277	0.133
51002.5660	0.6894	−27.4	0.1	−1.113	0.113	0.284	0.124
51288.5618	0.3234	15.8	0.7	—[a]		—	
51332.5522	0.7285	−30.1	0.4	−1.316	0.127	0.068	0.140
51381.4301	0.1787	14.9	0.5	−0.925	0.117	0.610	0.129
51382.4819	0.1884	16.1	0.6	−1.019	0.096	0.375	0.105
51383.3908	0.1968	16.2	0.6	−1.186	0.104	0.287	0.114
51385.4111	0.2154	17.6	0.5	−1.342	0.082	0.208	0.090
51386.3445	0.2240	18.0	0.5	−1.353	0.104	0.158	0.115
51387.3975	0.2337	17.7	0.5	−1.285	0.063	0.135	0.069
51387.4260	0.2339	17.7	0.5	−1.325	0.056	0.134	0.061
51388.3746	0.2427	18.4	0.5	−1.380	0.075	0.089	0.082
51407.6048	0.4198	4.0	0.6	−1.316	0.078	0.113	0.086
51417.5704	0.5115	−7.6	0.5	−0.475	0.154	0.876	0.169
51423.4962	0.5661	−16.5	0.4	−0.376	0.135	1.206	0.149
51426.4815	0.5936	−19.5	0.3	−0.750	0.087	0.607	0.096
51427.4105	0.6022	−20.9	0.4	−0.903	0.100	0.433	0.110
51465.4373	0.9524	−12.7	0.7	−1.009	0.105	0.542	0.116
51473.4580	0.0263	−3.5	0.7	−1.324	0.101	0.215	0.111
51474.2698	0.0337	−1.3	0.7	−1.387	0.076	0.153	0.083
51476.2680	0.0521	0.4	0.6	−1.342	0.069	0.160	0.076
51477.3756	0.0576	—	—	−1.259	0.067	0.207	0.074

[a] Ca II H & K.

The observed RV values are displayed as a function of the orbital phase, determined from our ephemeris (Eq. (1)), in Fig. 2. Adopting our conjunction time, the epoch of Hall et al. (1990a), JD = 2445988.0, appears to be shifted by half a period, i.e. this light-curve minimum epoch corresponds to the conjunction with the hot secondary star in front instead of the cool primary star, as they assumed. The epoch of the deeper minimum observed by Barksdale et al. (1985) is in good agreement with our ephemeris.

Following Lucy & Sweeney (1971), we have assumed circular orbits and deduced new orbital parameters from our own radial velocities. The best fit orbital solution for the cooler component is reported in Table 2.

Table 2. Orbital parameters for the cooler component of HR 7428.

Element	Present solution	Sanford solution
K_{c}	23.71 ± 0.10 $\mathrm{km\,s^{-1}}$	22.1 $\mathrm{km\,s^{-1}}$
γ_{c}	-5.85 ± 0.09 $\mathrm{km\,s^{-1}}$	−5.2 $\mathrm{km\,s^{-1}}$
T_{conj}	2450601.982 ± 0.138	2423455.2[1]
P	108.578 ± 0.005 days	108.5707 days
$a_{\mathrm{c}} \sin i$	$3.54 \times 10^7 \pm 0.02 \times 10^7$ km	3.304×10^7 km
$f(m)_{\mathrm{c}}$	0.1500 ± 0.0025 $M_\odot$	0.1222 $M_\odot$

[1] Deduced from the time of periastron passage.

The contribution of the hotter component to the observed spectrum becomes stronger at shorter wavelengths. With the aim of detecting the spectrum of the hot component we have taken an exposure of HR 7428 in the blue-violet region with our spectrograph, equipped with the thinned back-illuminated UV-enhanced SITe CCD. We recorded 11 echelle orders with a complete wavelength coverage from 4550 Å to 3700 Å. Spectra of α Boo and α Lyr

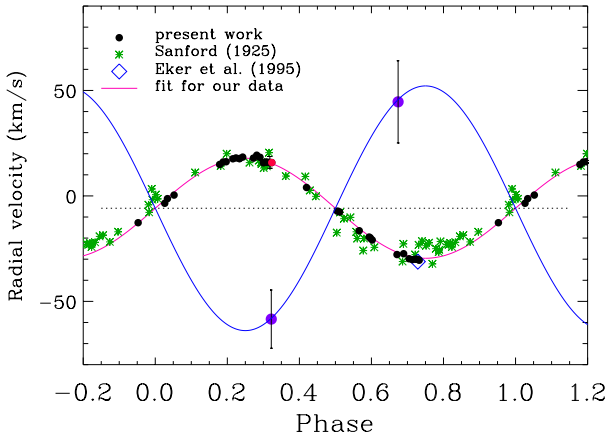

Fig. 2. Radial velocities of HR 7428 and circular solution. Our own data are displayed with filled circles. Other symbols represent literature RV data, not used for the orbital solution. Two radial velocity measurements for the hot star, from our own blue-violet spectrum ($\phi = 0.32$) and from an IUE high resolution spectrum ($\phi = 0.67$), are also shown together with a tentative orbital solution for this component.

(which mimic the cool and hot component of HR 7428, respectively) were obtained on the same night and with the same instrumental setting. Our purpose was to obtain the hot star spectrum by removing, from the observed spectrum of HR 7428, the weighted contribution of the cooler component simulated by the rotationally broadened spectrum of α Boo.

Due to the low S/N ratio of HR 7428 spectrum at these wavelengths, the residual spectrum is rather noisy, but clearly shows the typical signatures of a hot star, like the strong and wide Balmer lines. The residual spectrum in the wavelength region containing the three strong Balmer lines H_9, H_{10} and H_{11} ($\lambda\lambda 3835, 3798, 3771$) is shown in Fig. 3, superimposed on the spectrum of Vega obtained with the same instrument.

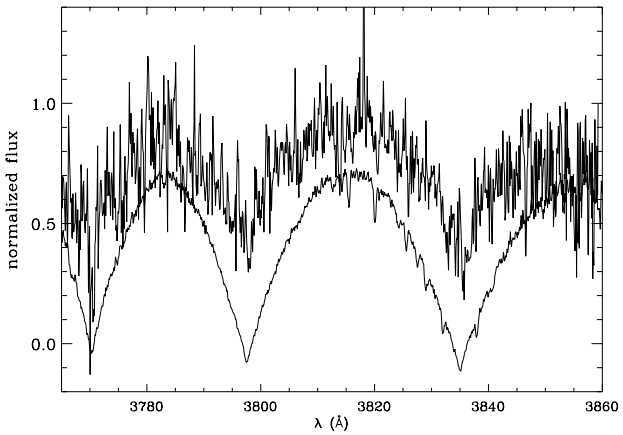

Fig. 3. Residual spectrum of the hot component of HR 7428 in the violet region, obtained as described in the text. The spectrum of Vega shifted downward by 0.2 units is displayed for comparison. The three hydrogen Balmer lines H_9, H_{10} and H_{11} are clearly visible.

We have cross-correlated the orders of the residual spectrum containing the strongest lines with the corresponding ones of Vega to find the radial velocity of the hotter component at this phase ($\phi = 0.322$). The evaluated radial velocity (-58 km s^{-1}) has a rather large error (± 14 km s^{-1}) because of the noise and of the large width of the hydrogen lines.

Another possibility for measuring the radial velocity of the hot component is to look for spectral signatures of the A2 star in high resolution IUE spectra. Unfortunately, no high resolution spectrum at short wavelengths (where the A2 star flux overcomes that of the cooler companion) is available. However, we could use the well exposed part of the long-wavelength region of spectrum LWR10313, acquired with IUE on 1981 April 8th ($\phi = 0.67$) and retrieved from the IUE Final Archive. We have also retrieved the spectrum LWR09830 of Vega, acquired nearly at the same time.

By cross-correlation of each order of the HR 7428 spectrum with the corresponding one of Vega, we measured the radial velocity of the A2 star, obtaining $+45 \pm 19$ km s^{-1}. The large error is essentially due to the low S/N ratio.

With these two RV values, we are able to give, for the first time, a tentative orbital solution for the hot component.

The orbital parameters of the hot component, including the values of $m \sin^3 i$ we derived, are reported in Table 3.

Table 3. Orbital parameters of the hot component of HR 7428.

Element	Present solution
K_h	58 ± 8 km s^{-1}
$a_h \sin i$	$8.6 \times 10^7 \pm 1.2 \times 10^7$ km
$m_h \sin^3 i$	$1.8 \pm 0.4\ M_\odot$
$m_c \sin^3 i$	$4.4 \pm 1.5\ M_\odot$
m_c/m_h	2.40 ± 0.06

3.2. Physical parameters

Physical parameters of the components of HR 7428 are not yet well known. As a matter of fact the radius of 62 $R_\odot$ found by Hall (1990) for the cool primary component leads to a distance of about 600 pc (Rodonò et al. 1998) which is at odds with the value of 302 pc given by Charles (1994) and with that measured by Hipparcos spacecraft ($d = 323 \pm 52$ pc).

Difficulties in accounting for optical and infrared magnitudes adopting stellar parameters reported in the literature were encountered by comparing black body emission with observed photometric fluxes (Rodonò et al. 1998).

As a first step, we have checked the consistency of magnitudes and colours with the radius of the cool component

reported in the literature, by means of the Barnes–Evans relation (Barnes et al. 1976) between $(V-R)$ colour index, V magnitude and angular diameter ϕ for late type stars:

$$\log \phi = 0.4874 + 0.858(V-R) - 0.2V. \quad (2)$$

The $(V-R)$ colour index is more appropriate than $B-V$ because it is practically not affected by the light contribution from the hot star. Adopting $(V-R) = 0.95$ (Fernie 1983) and $V = 6.371$ (Rodonò et al. 1998) we obtain $\phi = 1.067$ milliarcsec and, from the Hipparcos distance, we find for the cool component radius, $R_{\rm cool} = 37\ R_\odot$, which is significantly smaller than the value reported by Hall (1990), who had used a larger value of $v \sin i$.

We made a more accurate determination of physical parameters by using *UBV* magnitudes given in the literature and low resolution IUE spectra, whose spectral region is essentially dominated by the hot component, comparing them with synthetic theoretical spectra.

We defined an average *observed* UV spectrum using the available highest S/N ratio spectra, namely LWP 27954 and LWP 30925 for the long wavelength region (1850–3350 Å) and SWP 50606 and SWP 50609 for the short wavelength region (1150–2000 Å), retrieved from the IUE Final Archive (Nichols & Linsky 1996).

IUE spectra, as well as optical photometry, have been corrected for interstellar extinction. The typical value of 1 magnitude per kilo-parsec for the interstellar extinction and the Hipparcos distance, adopted for the computations, lead to an extinction magnitude $A(\mathrm{V}) = 0\overset{\mathrm{m}}{.}32$. Assuming the standard reddening law $A(\mathrm{V}) = 3.1 \times E(B-V)$, a colour excess $E(B-V) = 0\overset{\mathrm{m}}{.}10$ has been derived. IUE spectra have been de-reddened according to the selective extinction function of Cardelli et al. (1989).

Synthetic spectra have been generated with the NextGen (Hauschildt et al. 1999a, 1999b) photosphere models for the hotter secondary and cool primary star. The bright cool star model was computed for this purpose by Dr. Peter H. Hauschildt, including a spherical symmetry solution (Hauschildt et al. 1999b).

Consistent with the previous estimates of spectral type and with our estimate of the mass, several models between $T_{\rm eff} = 8400$ K and 9400 K were considered for the hot component.

To take into account the uncertainties in the relation between spectral type and effective temperature of the cooler component, initially we considered models with $T_{\rm eff} = 4200$ K, 4400 K, and 4600 K. The first model turned out to be cooler and the last hotter for our observational data. Finally, in agreement with the accurate spectral type determination by Ginestet et al. (1999), two models of $T_{\rm eff} = 4400$ K, with $\log g = 1.5$, $[\mathrm{M/H}] = 0$, $M = 5\ M_\odot$ and with $\log g = 2$, $[\mathrm{M/H}] = 0$, $M = 4\ M_\odot$ respectively, were considered.

Since synthetic spectra give fluxes at the stellar surface, the comparison of models with observations has been made by scaling the result with the angular radii of the components and the distance.

Several iterations have been performed to find the model that gives the better fit to the IUE spectrum and optical photometry, allowing the stellar parameters to vary independently. However, some constraints have been placed and tests for consistency have been made.

The distance was fixed to the Hipparcos value and the effective temperature adopted for the cool component was checked to be consistent with the spectral type classification and spectral line behaviour.

The temperature of the hotter component was mainly constrained by the shape of the UV spectral region. The temperature and the radius of the cooler component are instead mainly linked to the near-UV and optical spectral distribution.

The errors in the effective temperatures have been estimated as the minimum $\Delta T_{\rm eff}$ value that gives appreciable difference with respect to the observed spectrum. Due to the evident mismatch in the flux distribution of the two models with $T_{\rm eff} = 4200$ and 4600 K with respect to the observed one, we can estimate an uncertainty in the temperature of the cooler component, smaller than 200 K, probably of 100–150 K. For the hot component, having a lower weight in the composite spectrum, an error $\Delta T_{\rm eff} \approx 200$ K is deduced from the UV spectral region.

To evaluate the uncertainties in the radii we have considered the two main sources of errors: the error in Hipparcos distance (±52 pc) and the accuracy of the correction for interstellar extinction. The accuracy of the de-reddening procedure is affected by both the intrinsic uncertainties in the $E(B-V)$ value and the errors in distance. We have evaluated the first one by assuming the standard deviation on colour excesses equal to the variance of the coefficients given by Johnson (1965) for different sky regions. We find that the dominant source of errors is the distance uncertainty.

The final best-fit stellar parameters are listed in Table 4 together with the estimated errors.

The errors in the parameters, listed in Table 4, do not include any intrinsic uncertainty for the synthetic spectra. However, Hauschildt et al. (1999a), from a comparison of their models with the observed UV and optical spectra of solar type stars and Vega, found discrepancies always smaller than a few percent in the continuum. This source of error should be thus negligible in comparison with the accuracy of the data themselves.

In Fig. 4 the spectrum obtained by summing the synthetic spectra for the hot and cool component, degraded to the IUE spectral resolution, is plotted superimposed on the IUE de-reddened spectrum (left) and on the *UBV* fluxes (right). In the latter case the synthetic spectrum was convolved with a Gaussian kernel having a semi-amplitude of 30 Å. The models displayed have $T_{\rm eff} = 9000$ K, $\log g = 4.0$ and $T_{\rm eff} = 4400$ K, $\log g = 2$ for hotter and cooler components, respectively. The radii which give the best fit to the observed spectrum are 2.25 $R_\odot$ and 40 $R_\odot$, respectively.

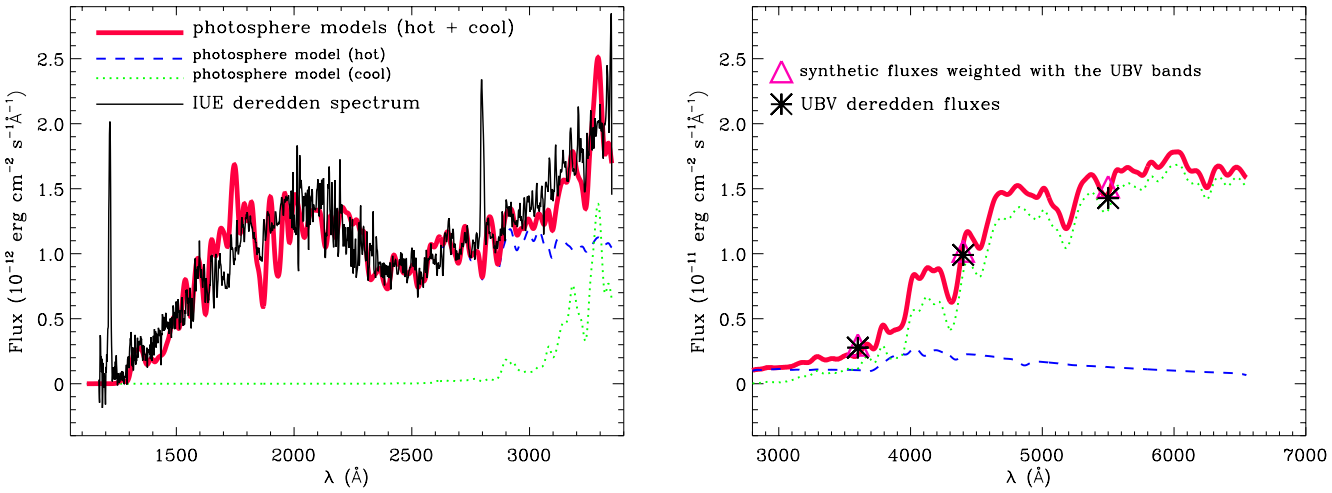

Fig. 4. Comparison of the photospheric models of the two components of HR 7428 with the IUE low resolution spectra (*left*) and *UBV* fluxes (*right*) at Earth. Both IUE spectra and optical photometry have been de-reddened with $E(B-V) = 0.10$. A distance of 322.6 pc, and radii of 2.25 and 40 $R_\odot$ for the hotter and cooler components respectively, are considered.

Table 4. Physical parameters of HR 7428.

Element	Primary (cooler)	Secondary (hotter)
R	$40.0 \pm 6.5\ R_\odot$	$2.25 \pm 0.50\ R_\odot$
$T_{\rm eff}$	$4400\ {\rm K} \pm 150\ {\rm K}$	$9000 \pm 200\ {\rm K}$
$\log g$	2.0 ± 0.5	4.0 ± 0.5

3.3. Rotational velocity and system inclination

The only measurements of the projected rotational velocity of HR 7428 that we found in the literature are $v \sin i = 21\ {\rm km\,s^{-1}}$ reported by Hui-song & Xue-fu (1987) and $v \sin i = 17.2\ {\rm km\,s^{-1}}$ measured by De Medeiros & Mayor (1995) with CORAVEL. Notwithstanding the moderate resolution, we have performed $v \sin i$ estimates on our spectra, taking advantage of the large number of observations and of the high S/N ratio. We have compared the echelle orders of HR 7428 centered at 6250 and 6400 Å with those of several slowly-rotating K-type giant stars, acquired with the same instrumentation. The standard stars that give the best reproduction of the HR 7428 spectrum are β Oph (K2 III) and α Ari (K2 III), whose $v \sin i$'s are negligible in comparison to the instrumental resolution.

We have set up a procedure for the $v \sin i$ determination. First we aligned in wavelength the spectra of the active and standard star by means of cross-correlation, then the spectrum of the standard star was progressively broadened by convolution with a rotational profile of increasing $v \sin i$. At each step, the sum of residuals between the observed and template spectrum was calculated and, at the end, the minimum of the residuals was found. The $v \sin i$ value that we deduced by analysing several HR 7428 spectra is $17.4 \pm 1.6\ {\rm km\,s^{-1}}$, in very good agreement with the CORAVEL measurement (De Medeiros & Mayor 1995).

The projected rotational velocity is given by

$$v \sin i = 2\pi R \sin i / P, \qquad (3)$$

where $P = 108\overset{\rm d}{.}8$ is the rotational period of the primary star from photometry (Hall et al. 1990a), and R is the radius from the model fit.

The system inclination that we derive from Eq. (3) with $v \sin i = 17.2\ {\rm km\,s^{-1}}$ is $i = 67°$. From the errors in radius (16%) and in $v \sin i$ (6%) we estimated the error in $\sin i$, which implies a system inclination in the 50°–75° range. The maximum inclination of 75° is constrained by the absence of eclipse in the HR 7428 light curve. Indeed, from radii and temperature that we determined (Table 4), a primary eclipse (hot star beyond) of $0\overset{\rm m}{.}07$ in V band and $0\overset{\rm m}{.}13$ in B should be observed. These inclination values lead to masses of the two components $M_{\rm H} = 2.75\ M_\odot$ and $M_{\rm C} = 6.71\ M_\odot$ for $i = 67°$, and $M_{\rm H} = 2.28\ M_\odot$ and $M_{\rm C} = 5.57\ M_\odot$ for $i = 75°$, while the lower limit of inclination (50°) would lead to higher masses not consistent with the spectral types.

3.4. Position in the HR diagram

Using the effective temperatures and radii in Table 4, we have placed the two components of HR 7428 on the $\log T - \log L$ plane. Their position and the evolutionary tracks for intermediate mass stars calculated by Fagotto et al. (1994) are displayed in Fig. 5.

The cool component lies in the region of He-burning stars, and implies a mass from 4 to 5 $M_\odot$, more consistent with the higher inclination limit, and an age from 140 to 150 Myr. The position of the hot component is consistent with a 2.3 $M_\odot$ star still on the main-sequence band, but slightly evolved. Its estimated age of 100–250 Myr is in perfect agreement with the estimated age of the cooler more massive component. This suggests a normal evolution of the two stars, yet without any relevant mass exchange, as expected from the long orbital period.

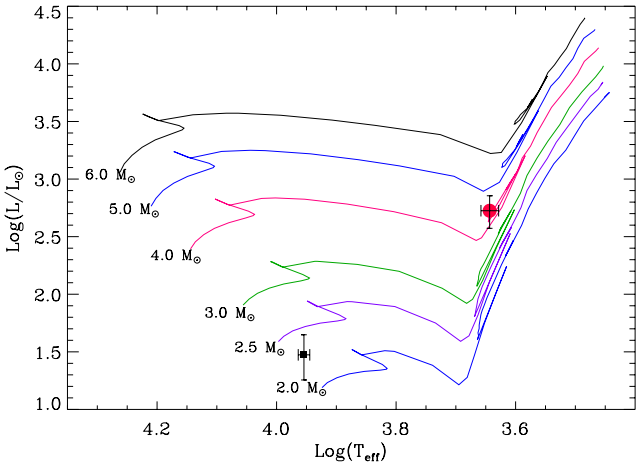

Fig. 5. Position of the cool (grey dot) and hot (black square) components of HR 7428 in a $\log T - \log L$ plane. The evolutionary tracks for different masses from Fagotto et al. (1994) are also shown.

4. Hipparcos photometry and ellipticity effect

The Hipparcos spacecraft has observed HR 7428 from December 1989 till March 1993.

The Hipparcos $H_{\rm p}$ photometric system is characterised by a response curve including B and V band and therefore not immediately comparable to classical UBV photometry.

The photometric data are shown in Fig. 6, where $H_{\rm p}$ magnitudes are plotted versus orbital phase computed with our new ephemeris. Notwithstanding the scatter of points, a photometric double wave appears well defined, with two maxima nearly at the quadratures and two minima nearly at the conjunctions. However, the behaviour is clearly asymmetric, the first maximum being brighter, with a peak at about phase 0.2. This behaviour is very similar to that observed by Strassmeier et al. (1989) from 1983 to 1984. These asymmetries were supposed to be connected to rotational modulation of starspots unevenly distributed on the surface of the K primary star. In a detailed study Hall et al. (1990a) show that the starspot wave, detected after removal of the variability produced by the ellipticity effect, is not permanent, and sometimes two different waves are simultaneously present.

To better define the starspot wave, we have calculated the light curve, dominated by the ellipticity effect, in absence of starspots, using the system parameters we derived in the previous sections.

Assuming a system inclination of 67°, we found a full amplitude of about $0\overset{\rm m}{.}02$, that is a bit smaller than the $0\overset{\rm m}{.}033$ value found by Hall et al. (1990a), and than the $0\overset{\rm m}{.}04$ value found by Strassmeier et al. (1989). A better agreement can be found with a higher inclination (near the maximum value of 75°) and a larger radius of the cool star (46 $R_\odot$) or with the minimum system separation allowed by the errors in $a_{\rm h} \sin^3 i$.

The residual asymmetry that appears in the difference between Hipparcos data and the ellipticity light curve solution may result from the presence of starspots, as suggested by Hall et al. (1990a).

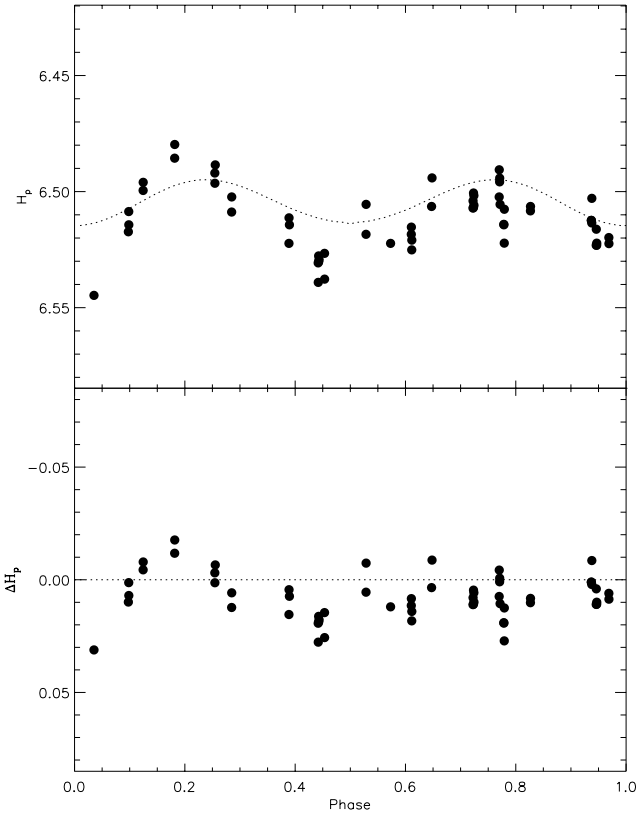

Fig. 6. *Top*: Hipparcos' magnitudes of HR 7428 through the period between 1989 and 1993, where the dashed line is the light curve solution accounting for the proximity effects. *Bottom*: Difference between Hipparcos magnitudes and the synthetic light curve.

5. Ca II H&K spectroscopy

In 1999 we have acquired a spectrum of HR 7428 in the blue-violet region. The Ca II H & K line region is shown in Fig. 7.

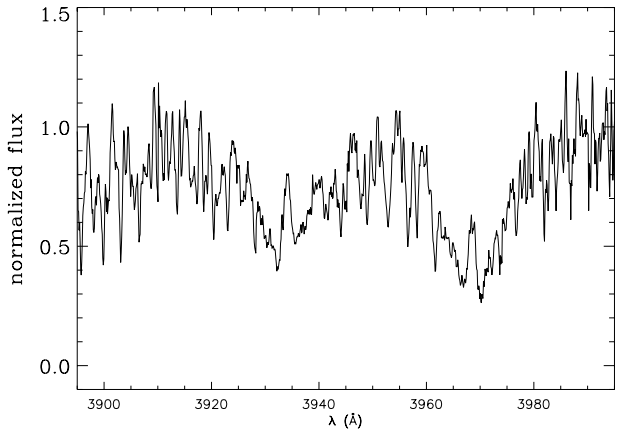

Fig. 7. CaII H & K lines in a spectrum of HR 7428 acquired in 1999.

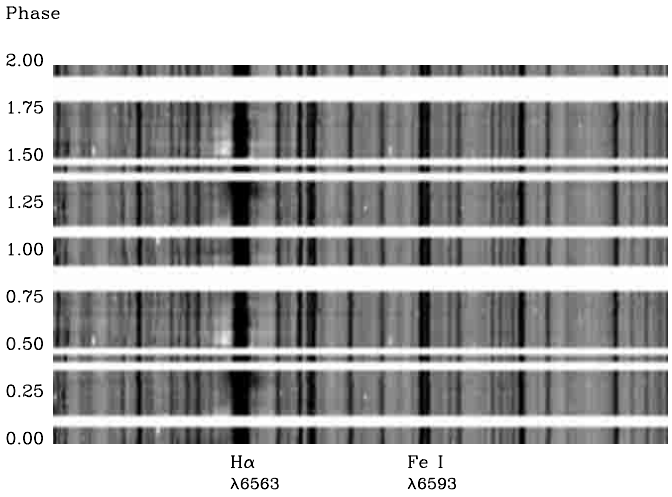

Fig. 8. Spectral image for the Hα order. All 32 spectra have been aligned on the velocity frame of the K2 star and normalized to the continuum. Orbital phase increases from 0 at the bottom to 1 in the middle and data are then repeated to have a better view of the variations with phase. The white rows correspond to phase intervals larger than 0.08 in which we have no spectra. Telluric H_2O lines display as sinusoidal features. The broad Hα extra-absorption feature around phase 0.3 and a blue-shifted emission component near phase 0.5 are apparent.

The chromospheric emission core is evident both in H and K lines. These emission components are broad, as expected from the Wilson-Bappu effect for a low gravity star (Elgarøy et al. 1997).

The absorption wings of the Ca II H line are deeper than those of the K line, due to the broad and stron hydrogen Hϵ absorption line of the hot component that is superimposed on the Ca II H line. Furthermore, the asymmetry seen into the K line core is probably due to the sharp K line absorption of the hot component spectrum that is blue-shifted at the time of the observation ($\phi = 0.323$).

The observed profiles are similar to those observed by Fernández-Figueroa et al. (1994), but in their spectrum the K-line core absorption is slightly red-shifted.

6. The Hα line behaviour

The Hα line appears significantly variable in width, intensity and shape.

In Fig. 8 all the spectra of HR 7428 we have obtained in the Hα region are shown, in orbital-phase order, as a trailed spectral image. In particular, from inspection of Fig. 8, variable broad absorption and emission components (red-shifted and blue-shifted, respectively) are apparent around the Hα absorption line of the K2 II-III star.

6.1. The difference profile behaviour

In order to analyze the behaviour of the Hα feature in more detail, we have used the technique of spectral subtraction. The standard low-active star α Ari, whose spectral type (K2 III) is very similar to that of the cool component of HR 7428, has been used to provide a "normal" Hα template.

In the synthesis of the "inactive template" we have neglected the contribution of the hot component because, according to the spectral model fit developed in Sect. 3.2, its weight to the total flux in the Hα region is only 4%.

The difference Hα profile, obtained with the spectral subtraction, therefore represents the contribution from the chromosphere of the K2 II-III star and from circumstellar material (see e.g. Richards 1992; Frasca et al. 2000).

Figure 9, left panel, displays a sample of observed spectra with superimposed the spectrum of α Ari artificially broadened to $v \sin i = 17.2\ \mathrm{km\,s^{-1}}$ (De Medeiros & Mayor 1995). The difference of the observed profile with that of the reference star α Ari, right panel of Fig. 9, displays a complicated structured profile. The Hα line core appears always filled-in with emission, and, in many cases, emission and/or absorption excess is present in the line wings. We can distinguish three typical situations:

a) normal wings and filled-in core, with the difference showing only a narrow central emission;
b) emission wings and filled-in core which lead to a difference profile with emission broad wings and a narrow central emission peak separated by absorption features on both sides;
c) broad absorption wings and filled-in core, which produce an emission core inside broad absorption wings in the difference profile.

In particular, nearly all the spectra between $\phi = 0\overset{p}{.}50$ and $\phi = 0\overset{p}{.}70$ show emission wings, with the blue side generally brighter than the red one. The spectrum at phase $3\overset{p}{.}50$ shows excess emission on the red wing with a profile very similar to that observed by Xue-fu & Hui-song (1984) in 1983 at the same phase. Since our spectra taken in the three years at similar phases also show similar profiles, it clearly appears that this wing excess emission is related to the orbital phase. Also, the excess absorption in both wings appears to be related to the orbital phase. Starting at phase $0\overset{p}{.}2$, a broad absorption wing progressively develops and reaches maximum strength near phase $0\overset{p}{.}30$–$0\overset{p}{.}32$. This effect almost completely disappears at phase $0\overset{p}{.}42$, when the blue wing has a normal shape and the red wing still displays some absorption.

We have taken a great care in the reduction process to avoid bias in the normalization procedure. The blazing function in the spectra has been accurately cancelled by the flat-field division, and the normalization has been made by selecting the continuum peaks outside the Hα wings (10–15 Å far away from the line center) and by interpolating the continuum-fitting polynomial function in the Hα line region. Therefore we conclude that the observed excess emission and absorption are intrinsic to the system.

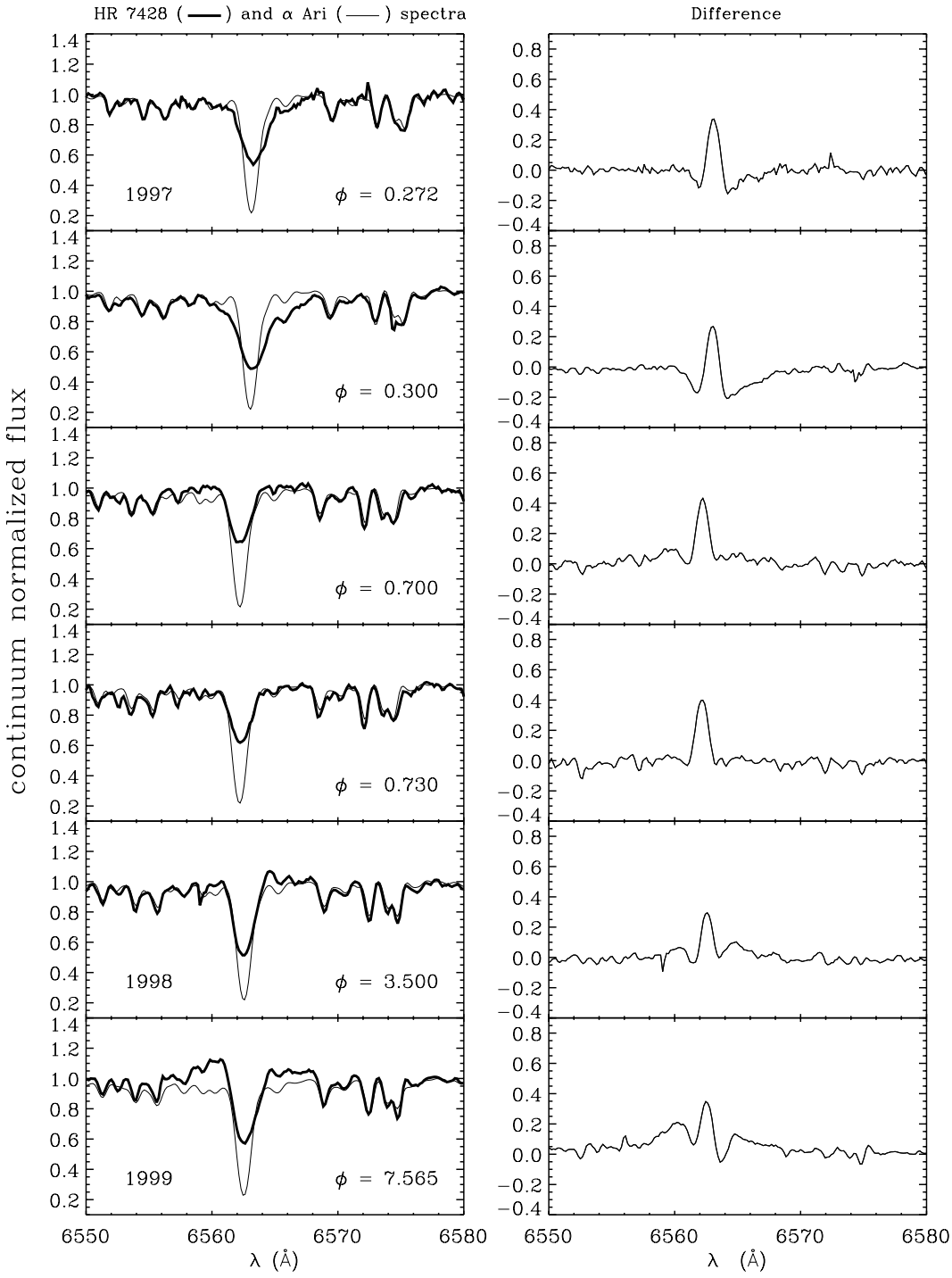

Fig. 9. A sample of spectra of HR 7428 (thick lines) compared to the rotationally broadened spectra of α Ari (thin lines).

6.2. The integrated equivalent width

Such excess emission and/or absorption is not easily interpreted in terms of chromospheric activity. Broad Hα emission wings are sometimes observed in RS CVn binaries. The phenomenon is always associated with transient events like strong flares (Catalano & Frasca 1994; Foing et al. 1994) or intense active regions, but also the line core fills in with emission and the overall profile appears to be composed of a narrow bright emission component and a broad fainter one (Montes et al. 1997, 2000; Lanzafame et al. 2000).

Although this Hα behaviour is difficult to ascribe to chromospheric inhomogeneities and may arise from circumstellar matter, as we will propose below, a chromospheric emission component should be present in the Hα profile, as suggested by the Ca II emission shown in Fig. 7 (see also Fernández-Figueroa et al. 1994), and by the Mg II h and k emission. We have re-determined, from archive IUE spectra, a Mg II flux $F_{\mathrm{Mg\ II}} = 2.38 \times 10^6\,\mathrm{erg\,s^{-1}\,cm^{-2}}$

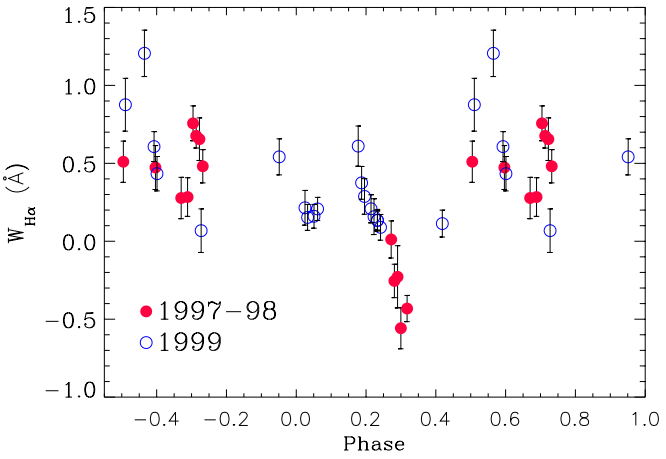

Fig. 10. Equivalent width of net Hα.

at the stellar surface, and then, according to the average correlation between Hα and Mg II emission established by Frasca & Catalano (1994), we estimate an expected net Hα equivalent width of 0.2 Å.

We have determined, from the difference spectra, the excess Hα equivalent width ($EW_{\rm H\alpha}$) by integrating the difference profile including the extended wings. Values are displayed in Fig. 10 including error bars determined as the product of the integration range and the $(S/N)^{-1}$ ratio, evaluated in two line-free windows selected on the residual spectrum at the two sides of the Hα line.

These measurements show a large spread, significantly greater than the estimated errors, with some intrinsic phase-dependent trend. In particular, the steady decrease from positive to negative values between phase 0.$^{\rm p}$2 and 0.$^{\rm p}$4 clearly reflects the development of the extended absorption wings. Fluctuation of the excess emission (positive values) reflects changes with phase and from cycle to cycle.

The average net Hα $EW \simeq 0.3$ Å measured between phase 0.$^{\rm p}$7 and 0.$^{\rm p}$2, when no excess emission or absorption is present, fairly well agrees with the expected chromospheric emission estimated from the Mg II emission flux. Emission EW values significantly larger than $\simeq$0.3 Å are found between phase 0.$^{\rm p}$5 and 0.$^{\rm p}$8 when the extended emission wings are present, thus we conclude that the real chromospheric Hα emission is at level of about $\simeq$0.3 Å. No emission modulation, ascribable to the rotation effect of inhomogeneous distribution of emission, can be distinguished.

6.3. The wing emission and absorption radial velocity

The emission wing profile, even if of lower intensity, is quite similar to that observed in shell stars (Marlborough & Cowley 1974) or in mass-losing red giants (Cacciari & Freeman 1983) as well as in the spectrum of the supergiant component of the binary system ϵ Aurigae, which is supposed to have a ring-like structure of moving gaseous clouds. On the other hand, the extended absorption wing

Table 5. Velocity shift of the broad extra-absorption and wing-emission centroid with respect the K star velocity, and the full width half maximum of the feature.

HJD −2440000	Phase	Feature	Vel. Shift km s^{-1}	Vel. disp. km s^{-1}
1385.4111	0.2154	Abs.	11.2	49.2
1386.3447	0.2240	Abs.	12.6	54.5
1387.3975	0.2337	Abs.	4.6	50.8
1387.4258	0.2339	Abs.	4.3	55.2
1388.3750	0.2427	Abs.	1.0	59.1
631.5586	0.2724	Abs.	20.8	89.6
632.5635	0.2817	Abs.	28.1	125.3
633.5440	0.2907	Abs.	31.9	115.9
634.5732	0.3002	Abs.	43.6	136.6
636.5156	0.3181	Abs.	12.4	99.4
1407.6045	0.4198	Abs.	18.7	51.3
982.5674	0.5052	Em.	15.0	108.1
1417.5703	0.5115	Em.	−41.7	133.2
1423.4961	0.5661	Em.	−23.5	174.0
1426.4814	0.5936	Em.	−31.5	146.1
1427.4102	0.6022	Em.	−44.6	133.8
1000.5713	0.6710	Em.	−16.0	87.9
1002.5664	0.6894	Em.	−16.8	89.8
678.4854	0.7046	Em.	−11.3	144.5
679.4756	0.7137	Em.	−5.4	101.6
680.4775	0.7229	Em.	3.1	106.7
681.5195	0.7325	Em.	−2.0	104.7

profile seen between phase 0.$^{\rm p}$2 and 0.$^{\rm p}$3 closely resembles the extra absorption present in the Hβ line of the T Tau star SU Aur (Petrov et al. 1996), explained as the effect of simultaneous outflows and inflows of matter.

These similarities do suggest that some flow of matter can be responsible of the excess emission and absorption in HR 7428. Here we propose that a single cloud localized in the region between phase 0.$^{\rm p}$0 and 0.$^{\rm p}$5 can produce both the extra emission and extra absorption in the Hα wings. This cloud is mainly seen projected against the K star disk at phase 0.$^{\rm p}$2–0.$^{\rm p}$3 and produces the extra absorption in the Hα wing spectrum of that star. Between phase 0.$^{\rm p}$5 and 0.$^{\rm p}$75 we see the same cloud illuminated and excited by the A2 star and projected against the sky, so its contribution is an extra-emission, due to radiative recombinations and de-excitations.

Both the broad extra-emission and absorption components exhibit asymmetric profiles compared to the chromospheric excess emission line of the K2 II-III star, indicating a relative global motion of the cloud with respect to the star. To quantify this motion we have estimated the central wavelength positions of the extra emission/absorption by fitting Gaussian profiles to the broad components and to the sharp central emission in the difference spectrum (see Fig. 11 for the description). Measured velocity shifts of the broad component are reported in Table 5 together with the velocity dispersion derived from the $FWHM$ of the feature. From this table one sees the red-shifted behaviour of the extra-absorption feature, that reaches its maximum shift (44 km s^{-1}), intensity

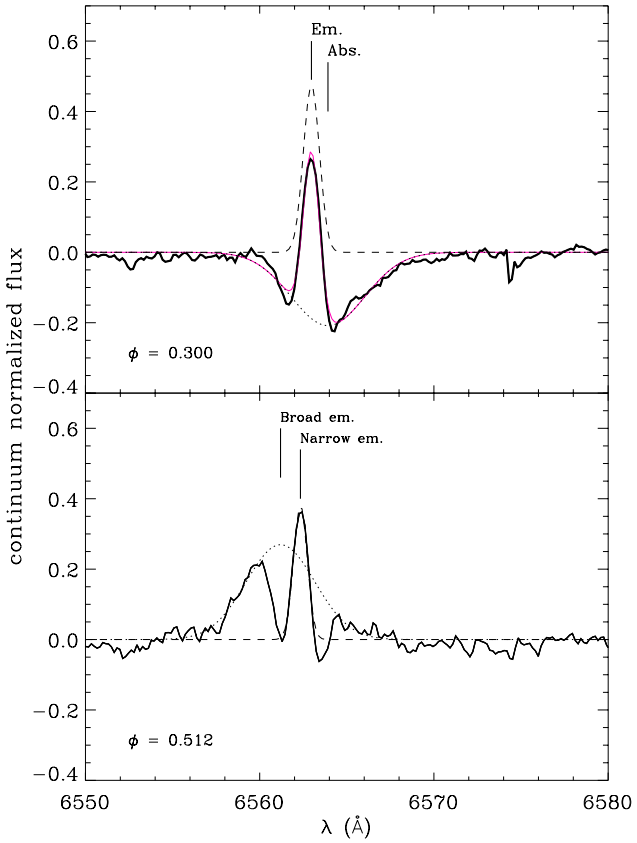

Fig. 11. Upper panel: simulation of the difference spectrum at phase $\phi = 0.30$ with the sum of two Gaussians, one for the broad extra-absorption (*dashed line*) and the other for the sharp core emission (*dotted line*). The thin line is the sum of the two fitting functions. Short vertical lines show the central positions for the two fitting functions. The red-shift of the extra-absorption component is evident. Although the red absorption wing is rather well fitted, we note that this simple function is not able to simulate the blue absorption wing. This indicates an asymmetric shape of the extra-absorption feature. **Lower panel:** example of fitting of Gaussians to the broad and narrow component for a spectrum showing excess wing emission.

and width at phase 0ᵖ.30. The broad emission component is instead mainly blue-shifted with respect to the K2 II-III star with a maximum of about 45 km s^{-1} at phase ≃0ᵖ.6.

The average *FWHM* of the broad components ranges from 50 to 140 km s^{-1} for the extra-absorption, and from about 90 to 150 km s^{-1} for the wing emission. This strengthens our hypothesis of a unique structure as being responsible for both the extra absorption and the wing-emission, with turbulent velocity of the order of 100–150 km s^{-1}.

7. Inter-system matter model

In Fig. 12 we plot the radial velocity of the components and of the broad absorption and emission features in the center of mass (CM) frame, as function of orbital phase. Although not strictly sinusoidal, the excess emission/absorption follows the orbital motion of the

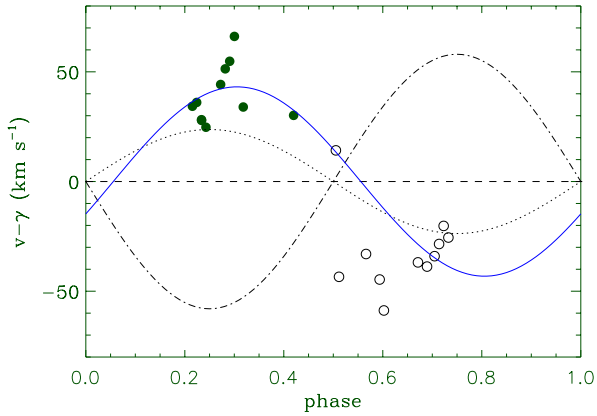

Fig. 12. Radial velocity of the extra-absorption (dots) and emission (open circles) in the barycentric rest frame. The dotted line is the *RV* curve of the K2 II-III star; the *RV* curve of the A2 star is also drawn (dash-dot line). The full line represents the *RV* curve of the extended region near the Roche-lobe limit of the K2 star (see Fig. 13).

K2 II-III star with a small phase shift and a larger amplitude, about 45–50 km s^{-1}. This does support our hypothesis that the emission/absorption features originate in a gas cloud placed somewhere within the system. If we assume that the system is fully synchronized, the location of such a cloud relative to the stars can be found from simple arguments.

Since the radial velocity of the supposed cloud is almost in phase with the K star, it should be located on the same side of that star with respect to the CM. Then the projected distance of the cloud is $a_{\rm cloud} = a_{\rm c}(K_{\rm cloud}/K_{\rm c})$, where $a_{\rm c} = a/(1+q)$, with q mass ratio and a the system separation, is the distance of the primary K star from the CM. $K_{\rm cloud}$ and $K_{\rm c}$ are the velocity semi-amplitudes of the cloud and of the cool star, respectively. Since the orbital solution gives $K_{\rm c} = 23.71$ and $(K_{\rm cloud}/K_{\rm c}) \sim 2$, then $a_{\rm cloud} \sim 7 \times 10^7$ km. From the radial velocity curves in Fig. 12 we can estimate a phase difference of ∼0ᵖ.1 with respect to the K2 II-III star, which means that the cloud should lie outside the line joining the centers of two stars in the direction of advancing phases. Since we see absorption effects on the cool star spectrum only for a limited phase interval (0ᵖ.2–0ᵖ.4), the material should have a limited extent and some thickness perpendicularly to the orbital plane, because the system inclination is smaller than 90°. According to the above estimate of the $a_{\rm cloud}$ distance and phase lag, the material seems to be located inside the Roche lobe of the cool star on the trailing hemisphere side.

The approximate location of the cloud is sketched as a shaded area in Fig. 13, where a scale model of HR 7428 is presented. Along the outer circle in Fig. 13, which indicates the position of the observer as a function of phase, the length of the arrows is proportional to the radial velocity of the broad emission/absorption feature in the CM rest frame.

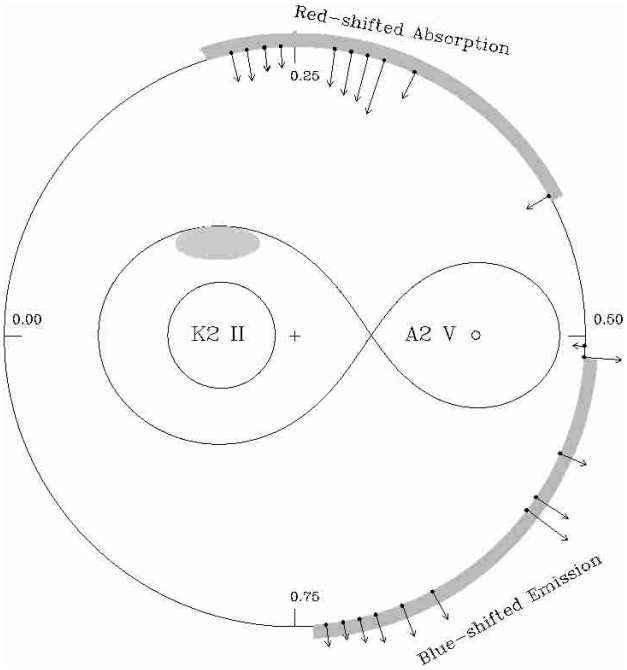

Fig. 13. Schematic model showing the Roche limit and the two components of the system in the orbital plane, as resulting from our solution. The cross indicates the center of mass of the system. The phase ranges of extra-absorption and broad emission features are stressed by thick grey lines. The possible location of the circumstellar region, responsible for the observed behaviour, is also showed as a shaded elliptical area.

8. Conclusions

HR 7428 has been included in our program of the Hα study of RS CVn binaries because photometric variability attributed to starspots (Hall et al. 1990a) and Hα variable emission (Cha et al. 1994) make this binary an interesting active system. Actually HR 7428 is not a typical RS CVn system but an unusual Algol-type system in which the evolved companion is not yet filling its Roche lobe and shows evident signs of magnetic activity.

In this work, in addition to the Hα chromospheric study, we have reached three main goals: i) we have determined new accurate orbital parameters; ii) we have given, for the first time, physical parameters of both components; iii) evidence for inter-system material has been inferred from the absorption/emission excesses in the Hα profile.

We have found that the Hα line behaviour is too complex to be explained simply in terms of chromospheric activity. However, we have isolated an excess emission in the line core that can reflect the chromospheric activity of the cool K2 II-III component. The average activity level corresponding to an Hα emission equivalent width $EW_{\mathrm{H}\alpha} \simeq 0.3$ Å is in agreement with the emission in the Mg II h & k and Ca II H & K lines, and as expected from the long rotation period of $108\overset{\mathrm{d}}{.}8$.

We have derived complete physical parameters of HR 7428, from new radial velocity data and spectral fit of the UV and optical spectrum. The hotter component has definitely been classified as an A2 V star a little evolved off the main sequence. The spectral model fit lead to a radius of about 40 $R_\odot$ for the cooler K2 II-III star. This value is significantly smaller than the previous value of 62 $R_\odot$ (Hall 1990), but also a little small to fully justify the observed photometric variations as an ellipticity effect.

The final values for the temperature and luminosity of the two components of the system place the hot component as a little-evolved main-sequence of about 2–3 $M_\odot$ and the cooler in the region of the He-burning stars, in agreement with the range of 4–5 $M_\odot$ we deduce from the orbital solution. The similar time evolution estimated for the individual components sets the age of the system in the range 100–200 Myr. This also indicates a normal independent evolution of the two stars, yet without any relevant mass exchange or mass loss. As a matter of fact the larger K2 II-III star is still well inside the relative Roche lobe as shown by the scaled diagram in Fig. 13, and no mass flow should be expected.

According to the orbital period and the system separation, the more massive component of HR 7428 should reach its Roche Lobe on the way to the red giant branch, leading to a case-C mass exchange. The evolutionary tracks by Fagotto et al. (1994) predict that the cool star will approach the Roche-lobe limit at an age of about 170 Myr, i.e. about 20 Myr after the present stage. From the Hα profile we have inferred the presence of inter-system material that seems to be accumulated mainly on the trailing hemisphere of the K2 II-III star, just near the edge of the lobe. From the width of the excess absorption/emission profile we estimate turbulent velocities in the cloud of up to 150 $\mathrm{km\,s^{-1}}$. Such velocities, very likely, could produce evaporation from the Roche Lobe and mass loss from the cool star.

The evaporated material is expected to accumulate in an envelope or ring around the system. The presence of circumstellar material around HR 7428 has been clearly detected from ISO observations. Rodonò et al. (1998) found significant IR excess at wavelengths greater than 1.6 μm with a definite inversion of the spectrum slope at 25 μm.

Since the K2 II-III star is still well inside its Roche lobe, the problem of the origin of the flowing mass arises. The magnetic activity does not appear able to produce extended loops or prominences, as sometime are observed in active systems like AR Lac (Frasca et al. 2000) or SS Boo (Hall et al. 1990b; Hall & Ramsey 1992) and therefore does not seem to be an appropriate mechanism to trigger a significant mass loss.

Evolutionary models including convection-overshooting predict for a 5 $M_\odot$ star a relevant mass loss at the present evolutionary stage of the HR 7428 cooler component. Models by Maeder & Meynet (1988) and Schaerer et al. (1993) predict mass loss rates of 5×10^{-9} or 10^{-8} $M_\odot\,\mathrm{year}^{-1}$ for stars of 4 or 5 solar masses in these evolutionary phases. Such mass loss rates could be responsible for the observed circumstellar effects like the extra-absorption/emission at Hα and the infrared excess. A more detailed model of the circumstellar material could

be attained with higher resolution spectra and a better phase coverage.

Acknowledgements. We wish to thank the Referee, Dr. D. S. Hall, for carefully reading the manuscript and for valuable comments. We would like to thank G. Carbonaro, A. Distefano, G. Occhipinti, and M. Puleo for valuable help in carrying out our observations. We are grateful to Dr. Peter Hauschildt for the atmosphere models he calculated for us. This work has been supported by the Italian *Ministero dell' Università e della Ricerca Scientifica e Tecnologica,* the *Gruppo Nazionale di Astronomia* of the CNR and by the *Regione Sicilia* which are gratefully acknowledged.

References

Barksdale, W. S., Boyd, L. J., Genet, R. M., et al. 1985, IBVS, 2737
Barnes, T. G., Evans, D. S., & Parsons, S. B. 1976, MNRAS, 174, 503
Bopp, B. W., & Talcott, J. C. 1978, AJ, 83, 1517
Cardelli, J. A., Clayton, G. C., & Mathis, J. S. 1989, ApJ, 345, 245
Cacciari, C., & Freeman, K. C. 1983, ApJ, 268, 185
Catalano, S., & Frasca, A. 1994, A&A, 287, 575
Cha, G.-W., Hui-song, T., Jun, X., & Yongsheng, L. 1994, A&A, 284, 874
Charles, P. A. 1983, in Activity in Red-Dwarf Stars, 71st IAU Coll., ed. P. B. Byrne, & M. Rodonò (D. Reidel Publ. Com.), 415
De Medeiros, J. R., & Mayor, M. 1995, A&A, 302, 745
Eker, Z., Hall, D. S., & Anderson, C. M. 1995, ApJS, 96, 581
Elgarøy, O., Engvold, O., & Joras, P. 1997, A&A, 326, 165
Evans, D. S. 1979, IAU Symp., 30, 57
Fagotto, F., Bressan, A., Bertelli, G., & Chiosi, C. 1994, A&AS, 104, 365
Fernández-Figueroa, M. J., Montes, D., De Castro, E., & Cornide, M. 1994, ApJS, 90, 433
Fernie, J. D. 1983, ApJS, 52, 7
Foing, B. H., Char, S., Ayres, T., et al. 1994, A&A, 292, 543
Frasca, A., & Catalano, S. 1994, A&A, 284, 883
Frasca, A., Marino, G., Catalano, S., & Marilli, E. 2000, A&A, 358, 1007
Ginestet, N., Carquillat, J. M., & Jaschek, C. 1999, A&AS, 134, 473
Gurzadyan, G. A. 1997, MNRAS, 290, 607
Gratton, L. 1950, ApJ, 111, 31
Johnson, H. L. 1965, ApJ, 141, 923
Hall, D. S. 1990, AJ, 100, 554
Hall, D. S., Gessner, S. E., Lines, H. C., & Lines, R. D. 1990a, AJ, 100, 2017
Hall, J. C., Huenemoerder, D. P., Ramsey, L. W., & Buzasi, D. L. 1990b, ApJ, 358, 610
Hall, J. C., & Ramsey, L. W. 1992, AJ, 104, 1942
Hauschildt, P. H., Allard, F., & Baron, E. 1999a, ApJ, 512, 377
Hauschildt, P. H., Allard, F., Ferguson, J. W., Baron, E., & Alexander, D. R. 1999b, ApJ, 525, 871
Hui-song, T., & Xue-fu, L. 1987, A&A, 172, 74
Lanzafame, A., Busà, E., & Rodonò, M. 2000, A&A, 362, 683
Lucy, L. B., & Sweeney, M. A. 1971, AJ, 76, 544
Maeder, A., & Meynet, G. 1988, A&AS, 76, 411
Marlborough, J. M., & Cowley, A. P. 1974, ApJ, 187, 99
Montes, D., Fernández-Figueroa, M. J., De Castro, E., & Sanz-Forcada, J. 1997, A&AS, 125, 263
Montes, D., Fernández-Figueroa, M. J., De Castro, E., et al. 2000, A&AS, 146, 103
Nichols, J. S., & Linsky, J. L. 1996, AJ, 111, 517
Parsons, S. B., & Ake, T. B. 1987, BAAS, 19, 708
Petrov, P. P., Gullbring, E., Ilyin I., et al. 1996, A&A, 314, 821
Richards, M. T. 1992, ApJ, 387, 329
Roberts, D. H., Lehár, J., & Dreher, J. W. 1986, AJ, 93, 968
Rodonò, M., Pagano, I., Cutispoto, G., et al. 1998, Ap&SS, 255, 237
Sanford, R. F. 1925, ApJ, 61, 320
Scargle, J. D. 1982, ApJ, 263, 835
Schaerer, D., Charbonnel, C., Meynet, G., Maeder, A., & Schaller, G. 1993 A&AS, 102, 339
Strassmeier, K. G., Hall, D. S., Boyd, L. J., & Genet, R. M. 1989, ApJS, 69, 141
Tonry, J., & Davis, M. 1979, AJ, 84, 1511
Xue-fu, L., & Hui-song, T. 1984, Inf. Bull. Var. Stars, 2606
Xue-fu, L., & Hui-song, T. 1986a, Chin. Astron. Astrophys., 10, 221
Xue-fu, L., & Hui-song, T. 1986b, Acta Astron. Sinica, 27, 259